High resolution camera for mapping Titan's surface

Bianca Reinhardt

Jet Propulsion Laboratory, California Institute of Technology

Titan, Saturn's largest moon, has a dense atmosphere and is the only object besides Earth to have stable liquids at its surface. The Cassini/Huygens mission has revealed the extraordinary breadth of geological processes shaping its surface. Further study requires high resolution imaging of the surface, which is restrained by light absorption by methane and scattering from aerosols. The Visual and Infrared Mapping Spectrometer (VIMS) onboard the Cassini spacecraft has demonstrated that Titan's surface can be observed within several windows in the near infrared, allowing us to process several regions in order to create a geological map and to determine the morphology. Specular reflections monitored on the lakes of the North Pole show little scattering at 5 microns, which, combined with the present study of Titan's northern pole area, refutes the paradigm that only radar can achieve high resolution mapping of the surface. The present data allowed us to monitor the evolution of lakes, to identify additional lakes at the Northern Pole, to examine Titan's hypothesis of non-synchronous rotation and to analyze the albedo of the North Pole surface. Future missions to Titan could carry a camera with 5 micron detectors and a carbon fiber radiator for weight reduction.

I. Introduction and Motivation

Mapping Titan's surface requires high resolution imaging, which is limited by absorption by methane and scattering by aerosols. The main imaging instrumentation on the Cassini Spacecraft consists of the Synthetic Aperture Radar (SAR), which can acquire 500 m/pixel images, the Imaging Science Subsystem (ISS), the RADAR and the Visual and Infrared Mapping Spectrometer (VIMS). The Huygens probe, designed to enter Titans atmosphere in January 15th 2005 in the equatorial region, and to analyze clouds and surface, has shown that fluvial features require resolution on the order of 50 m/pixel. Expecting the probe to land on a liquid surface, images of the probe surprisingly show a solid surface of the landing site. The Radar instrument later detects lakes filled with stable liquids, consisting of liquid methane and ethane, mainly located in the northern hemisphere of Titan. In the northern pole area, the Imaging Sub System (ISS) discovered Kraken Mare (Turtle et al., 2010), the largest lake on Titan with shorelines at latitudes as low as 40 degs. The Synthetic Aperture Radar (SAR) instrument acquired high resolution paths over these areas, discovering tens of smaller lakes as well as two other large lakes named Punga Mare and Ligeia Mare (Stofan et al., 2007). The three large lakes cover each an area more than 100,000 km^2 (Hayes et al., 2008). The radar coverage is not complete and one pending question is whether Kraken Mare and Ligeia Mare are connected.

Since Saturn's equinox in August 2009, the North Pole is illuminated, as the opacity of the North polar hood is decreasing (LeMouelic et al., 2011). As a result, the northern lakes have become visible at optical wavelengths. This study focuses on the Visual and Infrared Mapping Spectrometer (VIMS) onboard the Cassini spacecraft, which has demonstrated that Titan's surface can be observed within

several windows in the near infrared, denying the paradigm, that only radar can penetrate the atmosphere and provide high-resolution images of the surface. The Visual and Infrared Mapping Spectrometer (VIMS) was given the opportunity to observe the northern lakes when Cassini was close to Titan during the T69 flyby in June 2010, obtaining three medium resolution images of the North Pole, as well as one high-resolution image of one of the largest lakes, Ligeia Mare.

The VIMS observed a specular reflection on the lakes at 5 microns (Stephan et al., 2009), which suggests that there is very little scattering at 5 microns in the North Pole Area and allows a global map of the lakes with a pixel size between 3 and 7 km. This observation encourages us to assess the potential of 5-micron imaging of Titan. The spatial windows through which VIMS can observe Titan's surface (Figure 1) have been defined as:

H1 = 0.917-0.95 µm
H2 = 1.065 µm
H3 = 1.278-1.262 µm
H4 = 1.54-1.557 µm
D1 = 1.98-2.08 µm
D2 = 2.63-2.82 µm
D3 = 4.9-5.11 µm

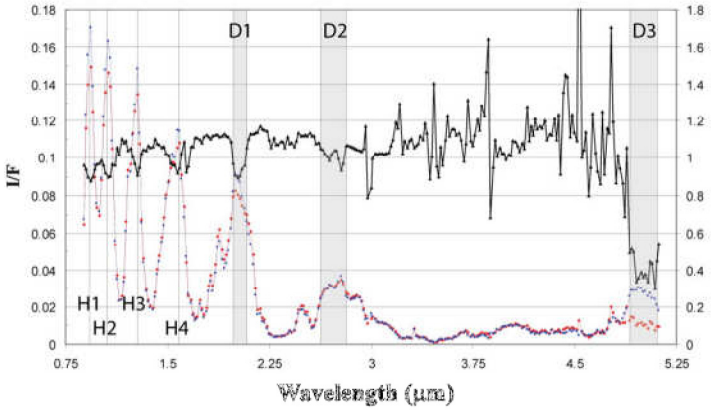

Figure 1. Spectra of the lake Ligeia (red line) and solid surface area (blue line) in cube IV. The ratio of the two is indicated by the dark line. The seven windows are indicated by the vertical lines and the three windows used in the present study are delineated in grey with D1, D2 and D3 being at 2 µm, 2.7 µm, and 5 µm, respectively.

The comparison between VIMS D3 and Radar images provide information on the evolution of the lakes between April 2007 and June 2010. It also constrains the valu of the orbital parameters including the amount of non-synchronous rotation (stiles et al. 2008).

The information of the ratio of radiance and irradiance, given by the VIMS camera, enables us to calculate the albedo for non-lake areas and determine the atmospheric contribution. Given these parameters further conclusions and constrains regarding the scattering by aerosols can be calculated.

By examining the images of several regions provided by the VIMS camera, it will be possible to give conclusions about the morphology and physical properties.

The study of Titans surface will consist of following regions:

- The North Pole Area
- Huygens landing site
- The Belet Dunes
- Tortola Facula
- The Ring feature

II. Methodology

A. Morphology

The Envi Software is used to process and analyze geospatial imagery. In combination with IDL, a programming language used for data analysis, it is possible to process the data received by the Cassini Space craft and to create a summation of detectors according to the defined observing windows D1, D2,

D3, H1, H2, H3 and H4, and to reproject these windows using certain map projections. The reprojected images can then be assembled producing a georeferenced mosaic of the surface, allowing the characterizations of surface features and morphology. Depending on the location of the observed area, certain projections are preferable. The North Pole area will be reprojected using the formulas of orthographic projection commonly used in cartography. For regions along the equator it is convenient to apply the Mercator projection, a cylindrical map projection.

With emphasis to the North Pole Area of Titan, it is of interest to further investigate the morphology of the observed lakes. Using Envi it is possible to link the optical properties such as radiance and irradiance to the geometrical properties, such as incidence, emission and phase angle, and longitude and latitude of each pixel, and surface properties. Then, regions of interests can be defined and characterized. These numbers can be exported to IDL as an array allowing calculations and graphs to determine the albedo of surface area, as well as location of specified features such as the small lakes in the northern hemisphere.

The albedo is defined as ratio of reflected radiation captured by the camera and radiation of the incident sun, and strongly depends on the frequency of radiation. By determining the albedo for defined frequencies, conclusions could be made regarding the scattered light by aerosols. It also provides information on the morphology (Soderblom et al., 2007), the composition (McCord et al., 2006), and the physical state (e.g. grain size, roughness) of the surface. Since there is no absorption at 5 micron, it is possible to determine the albedo for the solid surface in the North Pole area.

B. Scattering

The visibility of Titans surface is negatively influenced by light scattering by aerosols, strongly depending on the observing wavelength. The difference of visibility for the windows D1, D2 and D3 is shown in section 3.C. To estimate the amount of light penetrating the atmosphere and captured by the camera, it is necessary to understand the scattering components, which are effective for single scattering approximation. Since the emphasis lies on the window D3 with a mean wavelength of 5 micron, single scattering is of higher importance than multiple scattering. Giving the observed reflectance I of a planetary body with an atmosphere, therefore taking into account all single scattering components, following equation is defined as (e.g. Sobolev, 1975; Combes et al., 1991) and illustrated in figure 2:

$$I(\lambda,\phi) = F(\lambda)\cdot\cos(i)\cdot R_S(\lambda)\cdot e^{-\tau_i}\cdot e^{-\tau_e} \tag{1-1}$$

$$+F(\lambda).\omega_0\frac{f(\gamma)}{4}\frac{\tau_{atm}}{\cos(e)} \tag{1-2}$$

$$+F(\lambda)\frac{R_S'(\lambda).\omega_0.\tau_{atm}}{2}\int_0^1 p(\mu',\cos(i))d\mu' \tag{1-3}$$

$$+F(\lambda)\cos(i)\frac{R_S(\lambda).\omega_0}{2}\frac{\tau_{atm}}{\cos(e)}\int_0^1 p(\cos(e),\mu')d\mu' \tag{1-4}$$

$$+F(\lambda)R_S^2(\lambda).\omega_0.\tau_{atm}\int_0^1\left[\int_0^1 p(-\mu',\mu_0')d\mu_0'\right]d\mu' \tag{1-5}$$

with $p(\mu,\mu_0)=\frac{1}{2\pi}\int_0^{2\pi} f(\gamma)d\phi$

and $f(\gamma)=\frac{1-g^2}{(1+g^2-2g\cos\gamma)^{3/2}}$ known as the Henyey-Greenstein Phase Function normalized to 4π, in which γ = 180°- ϕ is the scattering angle, with μ=cos(e) and μ_0=cos(i), and cos(γ) defined as: $\cos(\gamma)=\mu\mu_0+\cos(\varphi)\sqrt{1-\mu^2}\sqrt{1-\mu_0^2}$

The parameters, which can be determined using Envi and IDL, and therefore are known, are:

$I(\lambda,\phi)/F(\lambda)$= Radiance/Irradiance
cos(i) = Cosine of incidence angle
cos(e) = Cosine of emission angle
γ = 180°- phase angle

Where as following parameters are unknown and can be constrained using the single scattering approximation equation:

$R_S(\lambda)$ = bidirectional reflectance of a perfect Lambertian surface

τ_{atm} = optical depth of the atmosphere ($0<\tau_{atm}<1$), depending on the scattering cross sections, density of scatterers, and height of the scatterers layer.

ω_0 = single scattering albedo ($0<\omega_0<1$)

$f(\gamma)$ = Henyey-Greenstein Phase Function, with -1<g<1:

g = single model parameter, known as the Henyey-Greenstein asymmetry factor and ranges between -1 and 1, in which negative values illustrate backscattering and positive values forward scattering. Isotropic scattering ranges around g=0 and represents mostly sideways scattering.

The first component (1-1) describes the direct light reflected by the surface considering the extinction by atmospheric scatterers. If τ_i and τ_e are small and ignoring the effect of sphericity, therefore are planar, with i and e small enough, then the term $e^{-\tau_i}\cdot e^{-\tau_e}\approx\left[1-\tau_{atm}\left(\frac{1}{\cos(i)}+\frac{1}{\cos(e)}\right)\right]$.

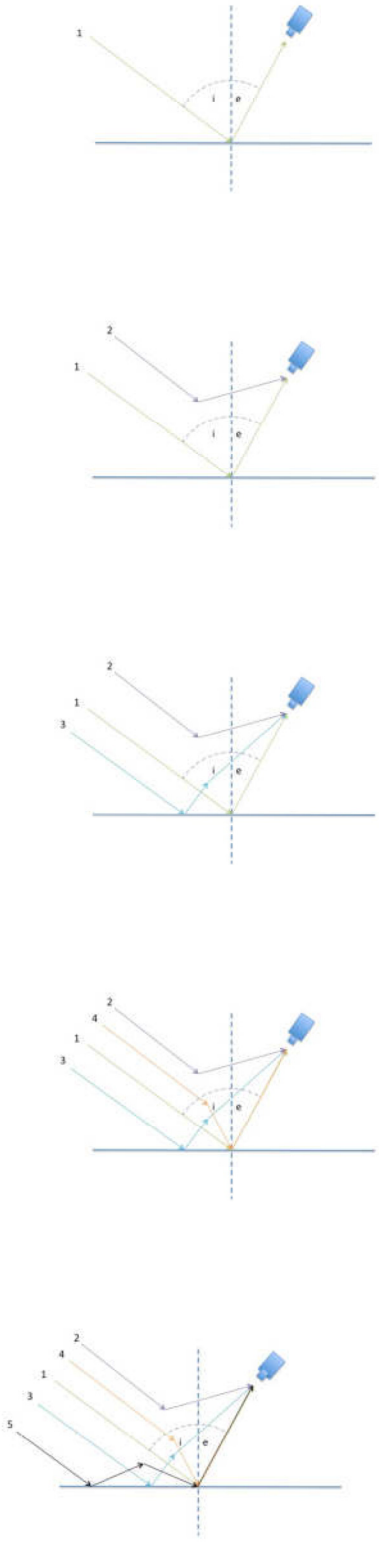

Figure 2. Effective single scattering approximation components

The second component (1-2) added to the direct light reflected by the surface, characterizes the light scattered to the camera before reaching the surface.

Assuming that the lakes act as mirrors with a specular reflection, and the bidirectional reflectance of the lake surface is zero, the only term affecting the observed reflectance of a lake is the light scattered by the atmosphere (1-2), which allows an estimation of the single scattering albedo such as the optical depth.

When monitoring the shoreline of Ligeia Mare a third scattering component (1-3) needs to be taken into account, which describes the light reflected from the surface and then scattered by the atmosphere to the camera, noting that R_S' is the bidirectional reflectance of the solid surface, where as R_S is the bidirectional reflectance of the lake's center, and therefore equal to zero, when observing the shoreline.

The reflected light by the solid surface is additionally influenced by a fourth (1-4) and fifth term (1-5), described as the light scattered by the atmosphere, then reflected by the surface to the camera, and the light reflected, scattered by the atmosphere back to the surface and anew reflected to the camera.

The fifth term (1-5) shows a squared bidirectional reflectance R_S, which suggests that this value is very small in comparison to the other terms and therefore can be neglected. The analysis of these terms with given values of the center of Ligeia Mare, at the shore line and at solid surface allows the modification of atmospheric properties and a deeper understanding of the scattering by aerosols of Titan's atmosphere.

III. Results

A. North Pole Area

After processing the received data of the VIMS Camera onboard the Cassini Space Craft with Envi, results show a geological map of the North Pole, consisting of three reprojected cubes (IV, V, VI) at 5 micron.

The image of the North Pole area (figure 3) clearly shows the lake Ligeia Mare including a very likely connection to Kraken Mare, which has not clearly been observed by RADAR. The small dark pixels on the VIMS image represent the small lakes (table 1 in the Appendix A), discovered and named in 2007 by RADAR. These feature observations show well-defined similarities to the RADAR image, which allows further investigations regarding surface feature changes, calculations of the synchronism of Titan's spin rate and analysis of the lakes. The comparison of the North Pole area at windows D1, D2, D3 and RADAR (figure 4) clearly presents the difference in resolution due to scattering of the atmosphere. While hardly any features can be observed in the windows D1 and D2, surface features are quite visible at D3, proving that there is barely scattering at 5 microns in the North Pole area.

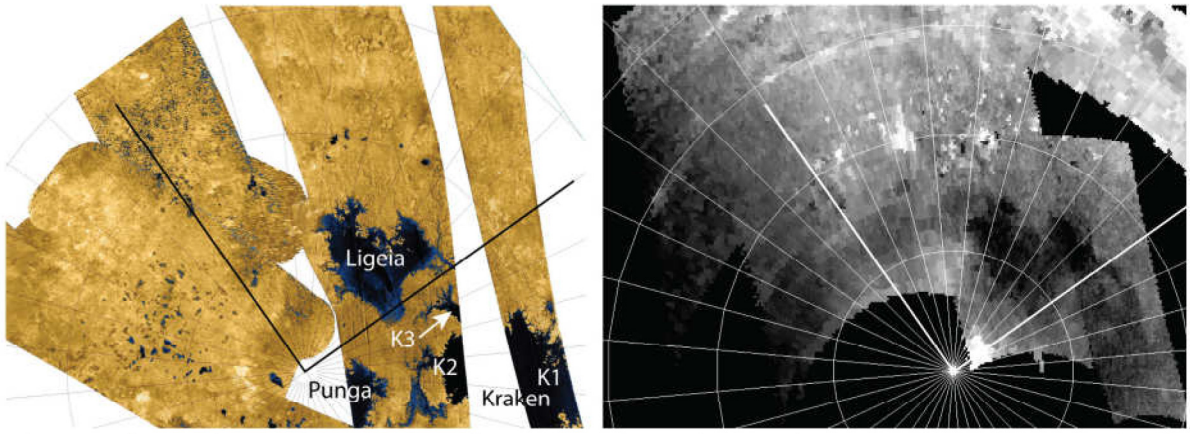

Figure 3. Comparison between the VIMS 5-µm mosaic obtained during T69 and the radar mosaic of this area. The longitudes 90 E and 180 are underlined to ease the interpretation.

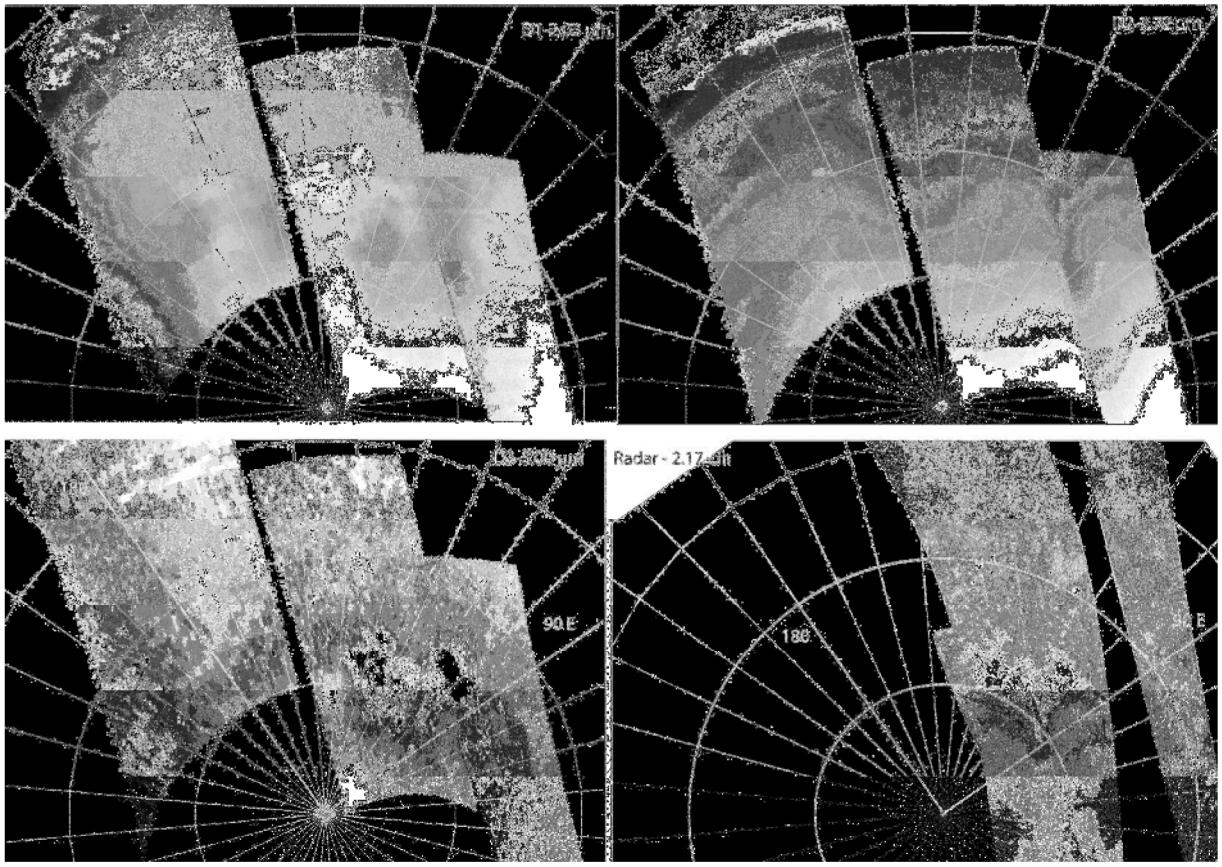

Figure 4. Mosaics of the three windows D1 (upper left), D2 (upper right), and D3 (lower left). These three mosaics can be compared with the radar map obtained by combining observations at T28 and T29 (lower right). Orthographic projections imply that the distance r on the map is proportional to sin(□) where □ is the colatitude defined as □ =d/R where d is the real distance from the pole along the meridian, and R is the Titan's radius. There is a clear correlation between surface features seen by radar and the D3 mosaic.

The VIMS mosaic shows additional surface area, not observed by RADAR, which made it possible to detect four new dark areas, assuming to be additional small lakes. One of them named VIMSNN3 on figure 5 actually corresponds to a partially filled lake for radar (Hayes, 2011). It suggests that the liquid layer is very thin and the 2.17 cm radar wave sees the lakebed through a very thin liquid layer. The three other dark spots, not mapped by RADAR, appearing in the longitude range 150-160, are named VIMSNN2, VIMSNN3, and VIMSNN4 and definitely correspond to additional lakes (table 2 in the Appendix A). During this study the IAU (International Astronomical Union) has named three of these lakes on the basis of the present observations to:

VIMSNN1 = Freeman
VIMSNN2 = Cardiel
VIMSNN3 = Towada

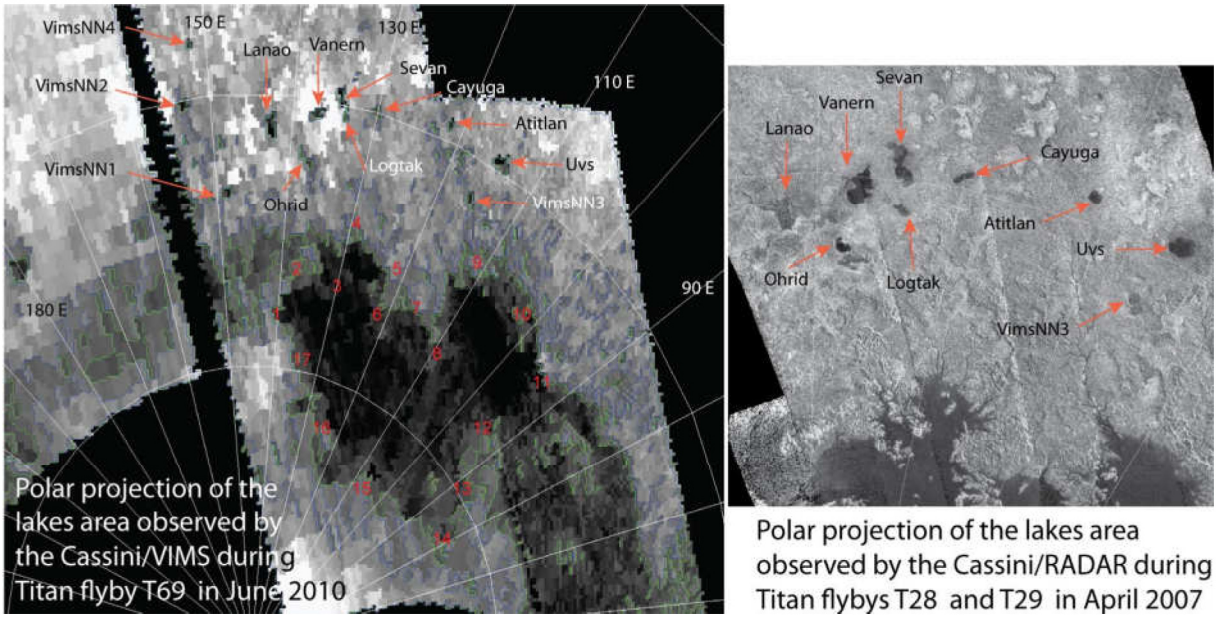

Figure 5. The small lakes on radar mosaic taken in April 2007 (right) and VIMS mosaic taken on June 2010(left).

The determination of the latitudes and longitudes of the center of small lakes show a standard deviation of 0.194° (8.7 km) and 0.264° (4.1 km) in latitude and longitude, in difference of position between the radar projection and the VIMS projection, which allows further calculations to test the hypothesis of non-synchronous rotation between April 2007 and June 2010. The observation also illustrates that the lakes are still filled with liquid since the radar observations and confirms Titan's obliquity of 0.3 deg (Stiles et al., 2009).

As mentioned above, the difference between the latitudes of the lakes has a standard deviation of 0.194° (8.7 km) and 0.264° (4.1 km) in latitude and longitude, respectively, which are on the order of the VIMS pixel size that is equal to 5.0 km and 7.3 km for cubes IV and V, respectively. It is worth noting that there is however a trend since the mean value of the difference between the VIMS coordinates and the Radar coordinates is equal to 0.137° and 0.250° for latitude and East longitude, respectively. That allows us to place an upper bound for a potential faster non-synchronous rotation of $2.3.10^{-4}$ °/day. This value is five times smaller than the value of 1.11 10^{-3} °/day reported by Stiles (2008) and 50% smaller than the corrected valued reported by Stiles et al. (2010).

To illustrate the shoreline of Ligeia Mare of the VIMS image, we added an I/F contour line to the image, which shows an I/F value of 0.27 for the borderline of the lake (figure 7).

Plotting Ligeia Mare's surface area of RADAR as a function of the levels I/F (figure 6) shows, this area is equal to a level of I/F=0.236 on the VIMS image. However, observations of the VIMS image demonstrate that the shoreline of Ligeia Mare exceeds the level of I/F=0.236, rather suggesting the shoreline to be suited at I/F=0.27.

An approach to estimate the area surface of Ligeia Mare is to determine a numerous amount

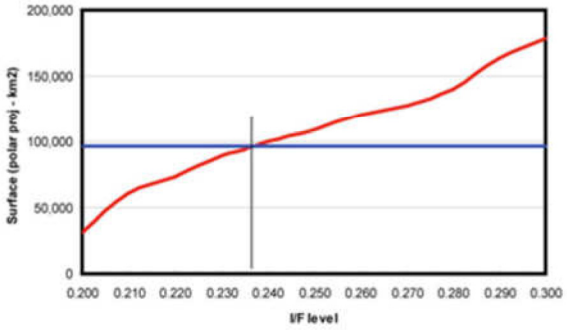

Figure 6. ENVI surface area of Ligeia Mare as a function of the I/F level

of shoreline coordinates and to display an outline of the shoreline in a graph for the levels 0.236 and 0.27. This allows an illustrative comparison to the shoreline estimated with RADAR using the same approach.

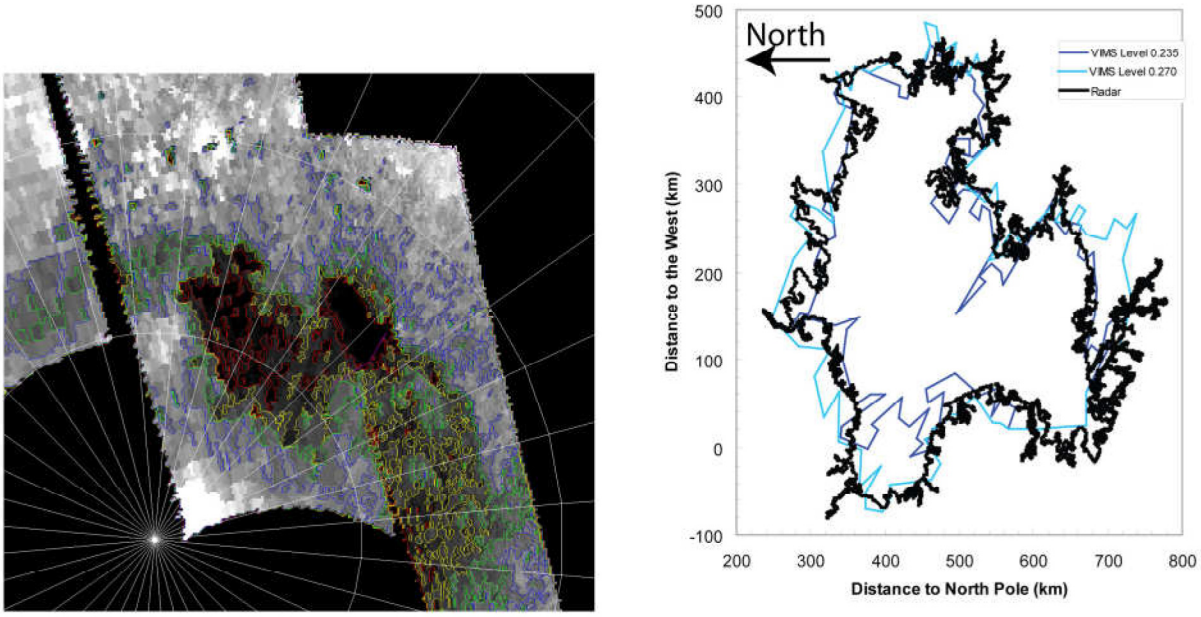

Figure 7. VIMS image of Ligeia Mare with I/F levels 0.2(red), 0.235(yellow), 0.27(green), 0.3 (blue) (left); Shoreline of Ligeia Mare obtained with VIMS at 0.235 and 0.27, and radar using Matlab (right)

The surface area calculations for the small lakes are not as accurate due to lower resolution. However an estimation of the lakes might be possible by determining I/F for every single pixel of the small lakes and it's surface surroundings. By defining values of I/F for liquid and non-liquid, permits the calculation of the percentage of lake and non-lake area for each pixel, assuming that the I/F value is a linear function of the (I/F) over a liquid surface (Ligeia) and the I/F over the solid surface.

Using the information given by the VIMS images for the North Pole area, it possible to constrain the albedo ($R_s(\lambda)$) of the solid surface at 5 micron, depending on the incidence angle. Keeping in mind that there is no absorption in the atmosphere at 5 micron (window D3). To do so, we plot I/F of the solid surface as a function of the Cosine of the incidence angle (figure 8). By applying a linear fit to the function, we receive a linear trend with a slope of 0.386, which corresponds to 2,757%. The y-axis intercept at cos(i) = 0 is the surface albedo, also equal to the surface albedo of he center of the lake, as described in section 3c.

The surface albedo value is also used to estimate the light scattered by the atmosphere in the North Pole Area, further discussed in section 3c

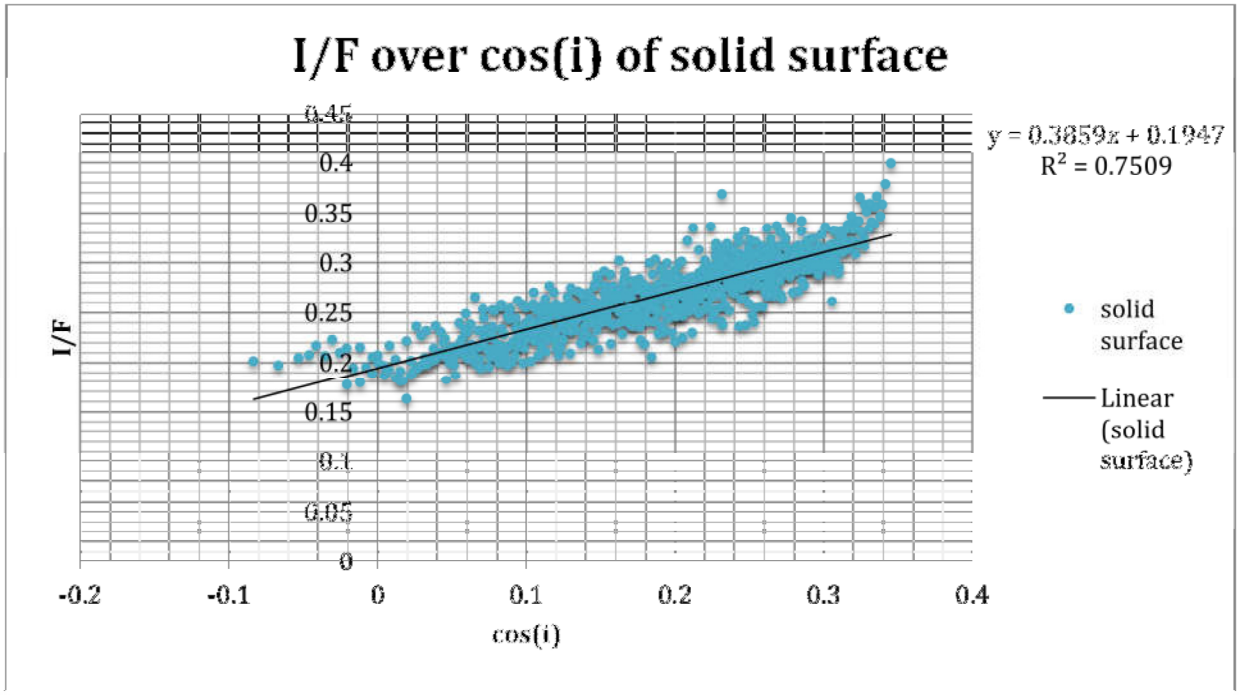

Figure 8. Graph of I/F of the solid surface as a function of the Cosine of incidence angle

B. Huygens Landing Site, Belet Dunes, Tortola Facula, Ring Feature

Besides studying the surface area of the North Pole, data of further areas have been processed to create geological maps and to analyze the resolution of these areas based on the windows D1, D2 and D3. The comparison between the three windows show, that the best resolution is at 2 micron (D1) and while the wavelength increases, the resolution is negatively influenced by the signal to noise ratio, very notable at 5 micron (figure9).

Huygens Landing Site

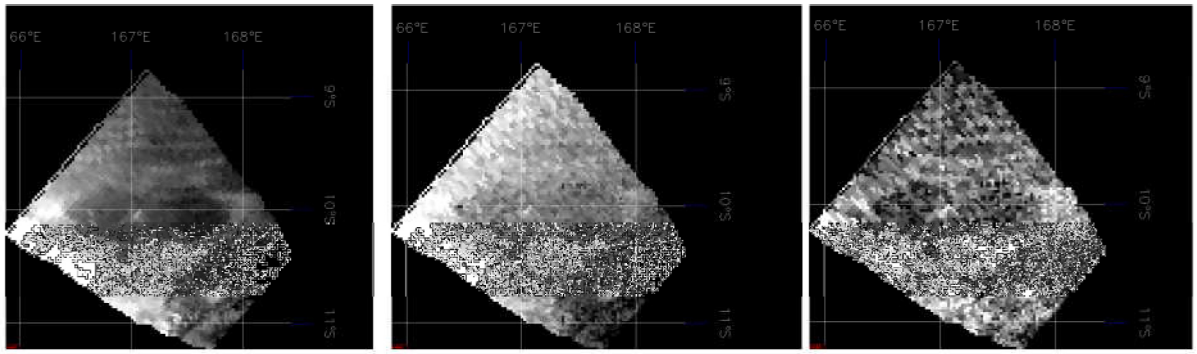

Figure 9. Comparison of Huygens landing site: D1(left), D2(center), D3(right)

A color image of the Huygens high-resolution image (figure 10) is gained by using the defined ratios, *red = H4/H3*, *green = D1/H3* and *blue = H3/H2*. To receive a better color image an estimated atmospheric contribution has been subtracted of each window, using IDL.

The created mosaics of the Belet Dunes, Tortola Facula, Ring Feature, for the windows D1, D2 and D3, as well as a complete mosaic of the covered surface area, obtained by VIMS, are presented in the Appendix B.

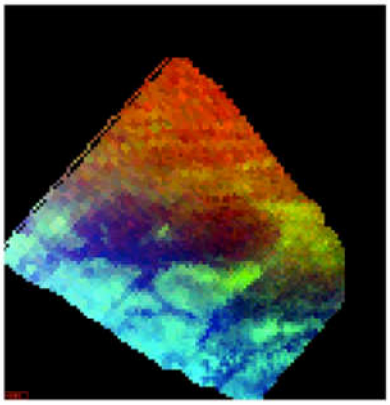

Figure 10. RGB image of Huygens landing site

C. Light Scattering by Aerosols

This section enhances further understanding of the light scattered by Titan's atmosphere in the North Pole area. Since we observe the surface area at larger wavelengths, single scattering is more significant than multiple scattering. Using the equation of single scattering approximation (1) (e.g. Sobolev, 1975; Combes et al., 1991), we can estimate several parameters affecting the penetration of light through the atmosphere. To do so, we examine the center and the shoreline of Ligeia Mare, such as the solid surface, and determine the values necessary to constrain the unknown parameters.

Center of Ligeia Mare: Assuming that the center of Ligeia Mare acts as mirror, the surface albedo should equal zero and the only component influencing the penetration of photons is the light scattered by the atmosphere to the instrument before reaching the surface. Therefore the equation reduces to:

$$I(\lambda,\phi) = F(\lambda).\omega_0 \frac{f(\gamma)}{4} \frac{\tau_{atm}}{\cos(e)}$$

Plotting the values of I/F for the center of Ligeia Mare as a function of the Cosine of the incidence angle (figure 11) proves clearly, that the reflection of photons does not depend on the incidence angle.

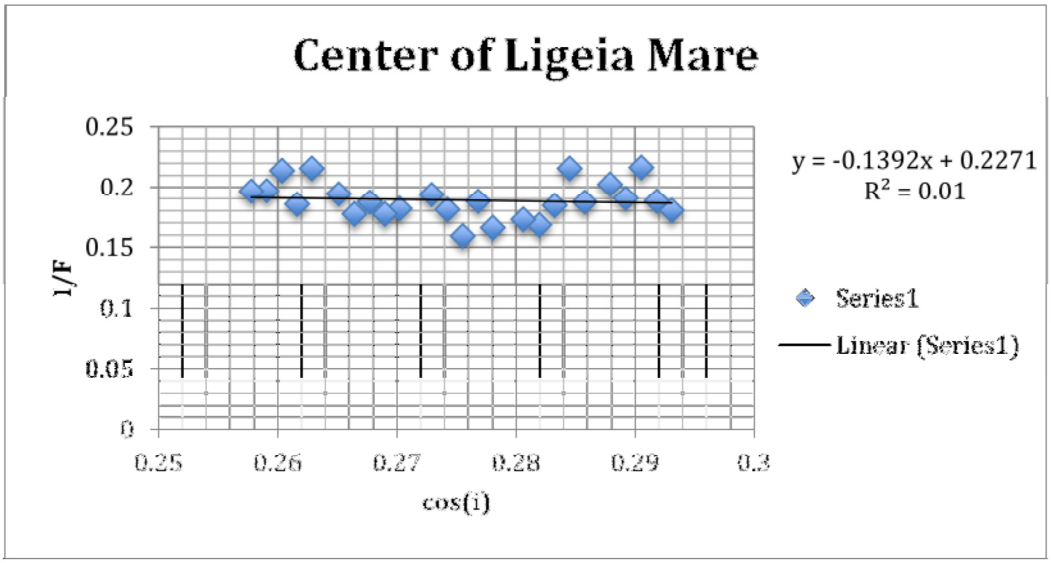

Figure 11. Graph of I/F of the Center of Ligeia Mare as a function of Cosine of incidence angle

The mean value for I/F is equal to 0.01348404, for one detector. This value, applied to the equation above therefore leads to:

$$0.01348404 = \omega_0 \frac{f(\gamma)}{4} \frac{\tau_{atm}}{\cos(e)} \quad \text{, with:} \qquad f(\gamma) = \frac{1-g^2}{(1+g^2-2g\cos\gamma)^{3/2}}$$

Given the mean value of the cosine of the emission angle, it is possible to constrain the unknown parameters τ_{atm}, ω_0 and g, as well as to illustrate the correlation between each other. The following graph (figure 12) shows the single scattering albedo ω_0 as a function of the Henyey-Greenstein Asymmetry Factor g, for different values of the optical depth of the atmosphere τ_{atm}, with

$$\omega_0 = 0.01348404 \cdot \frac{4}{f(\gamma)} \cdot \frac{0.312010724}{\tau_{atm}}$$

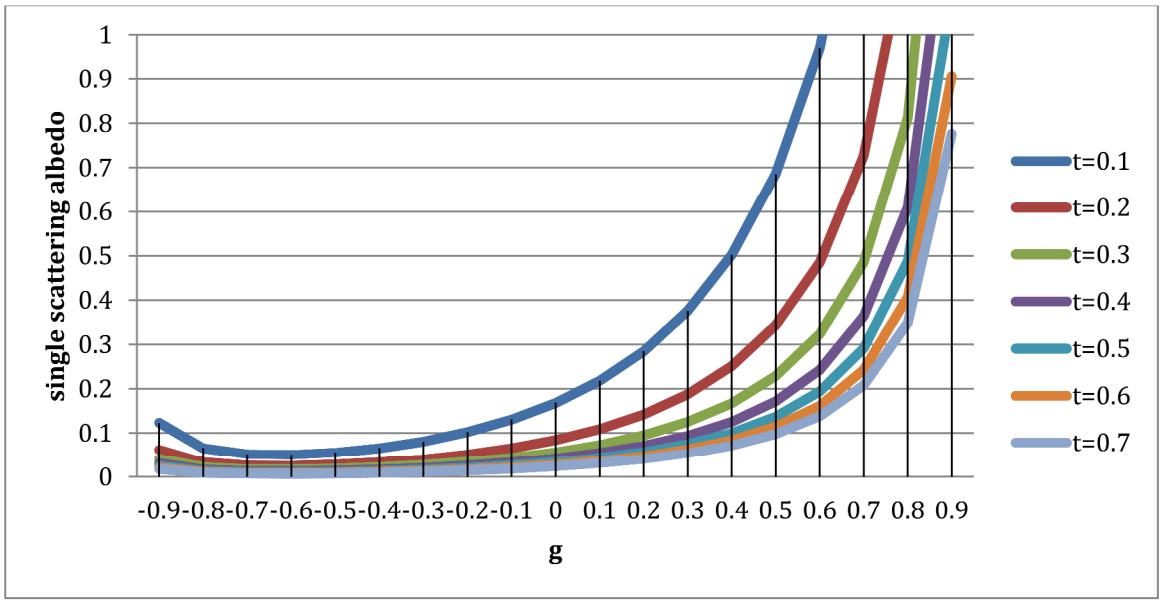

Figure 12. Single scattering albedo as a function of the Henyey-Greenstein Asymmetry Factor for differnet values of τ_{atm}

Since the observed scattering is mainly isotropic and forward scattering, values of g are of interest, which lie between 0 and 1. The graph also shows, that the single scattering albedo gets greater with smaller values of the optical depth of the atmosphere.

Shoreline of Ligeia Mare: When observing the shoreline of Ligeia Mare an additional scattering component has to be added to the equation, which includes the light reflected, then scattered by the atmosphere to the instrument. The bidirectional reflectance of the lake equals zero, which eliminates the first term. The only reflectance involved, is the albedo of the solid surface, which has been obtained in section 3.A. The effective equation of the shoreline leads to:

$$I(\lambda,\phi) = F(\lambda).\omega_0 \frac{f(\gamma)}{4} \frac{\tau_{atm}}{\cos(e)}$$

$$+F(\lambda)\frac{R_s^{'}(\lambda).\omega_0.\tau_{atm}}{2}\int_0^1 p(\mu',\cos(i))d\mu'$$

The plot of the I/F values for the shoreline as a function of the cosine of incidence angle (figure 13) show the independence of the incidence angle as well.

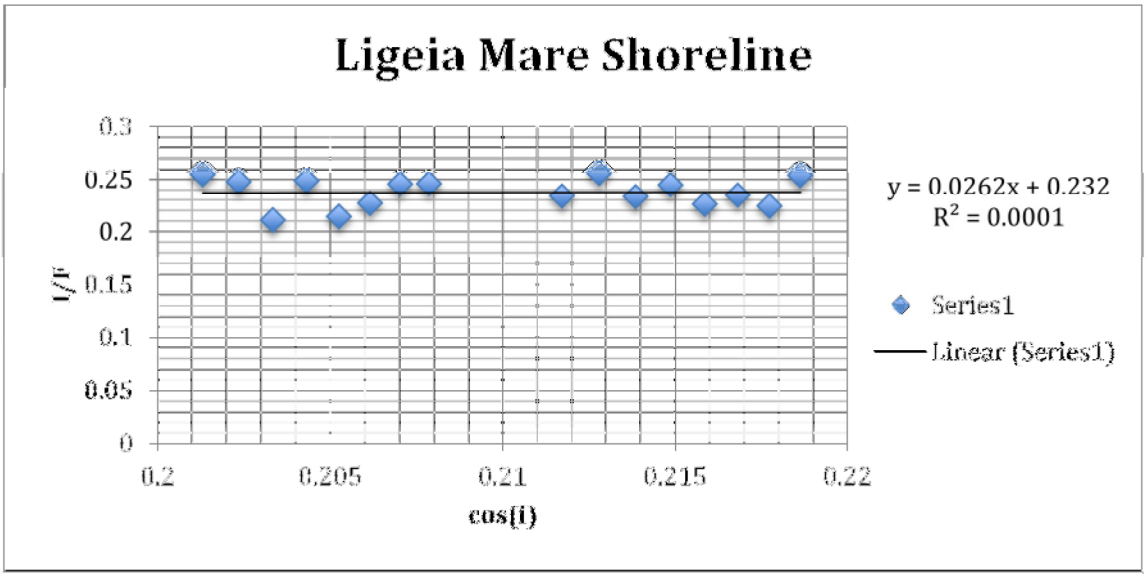

Figure 13. I/F of the shoreline of Ligeia Mare as a function of the cosine of incidence angle

The mean I/F value of the graph represents the second and third component of the equation:

$$0.01696346 = 0.01348404 + \frac{R_s'(\lambda).\omega_0.\tau_{atm}}{2}\int_0^1 p(\mu', \cos(i))d\mu'$$

$$\frac{R_s'(\lambda).\omega_0.\tau_{atm}}{2}\int_0^1 p(\mu', \cos(i))d\mu' = 0.00347942$$

The integral can be solved using Mathematica for different values of g and the mean value of the Cosine of incidence angle. The relation can be demonstrated by plotting the Integral as a function of g (figure 14).

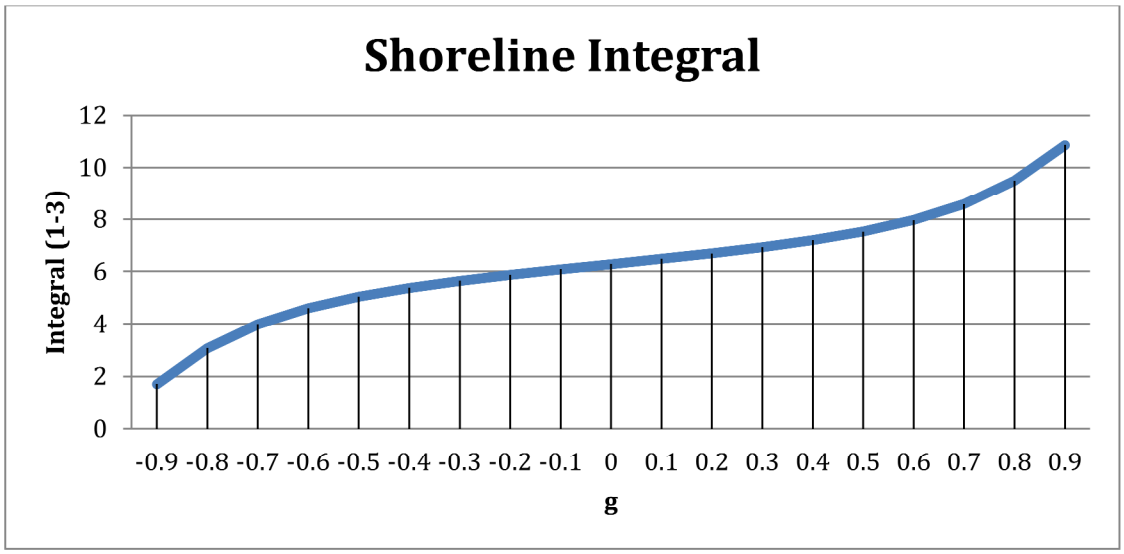

Figure 14. Integral (1-3) as a function of the Henyey-Greenstein Asymmetry Factor

Solid Surface:

When observing the solid surface of the North Pole area, all scattering components need to be taken into account to receive the overall scattering percentage. The plot in section 3.A reveals a fit of I/F as a linear function of the Cosine of incidence angle. The slope of the fit is calculated and has the value of 2.76%, which corresponds to the albedo of the solid surface. The total scattering proportion can be defined by the Y-axis intercept, which equals I/F = 0.1947 for the 14 channels of D3, and I/F = 0.0134 for a single channel, for cos(i) = 0. With increasing incidence angle, the I/F value increases linearly, showing the dependence of incidence angle for the solid surface, due to term (1-4) of the single scattering approximation.

The value of I/F at cos(i)=0 matches the I/F value of the center of the lake with a deviation of 3.125%.

IV. Discussion and Conclusion

This study has shown the high potential of the VIMS camera onboard the Cassini Space craft by receiving full visibility of Titan's North Pole Area at 5 microns, refuting the paradigm, that only radar can penetrate the atmosphere to receive images of Titan's surface. These observations allowed us to examine and analyze the morphology, such as geological changes during 2007 and 2010. Results show that there haven't been any major changes of surface features during these years. The analysis of the lakes enabled us to further understand the components of single scattering approximation, which can be used to develop a code modeling the limit in resolution, due to scattering, as a function of wavelength, in the next project phase.

To receive better images of the surface for further investigations, future missions to Titan should obtain a camera with 5 micron detectors to acquire high resolution images (50 m/pixel) of Titan's surface. To reduce the weight of the camera and therefore of the spacecraft, the camera could use a carbon fiber composite radiator. To receive the required heat conductivity, adjustments concerning size and material have to be made, influencing the weight of the radiator.

Acknowledgements

I would like to thank Christophe Sotin and Ken Lawrence for being wonderful mentors all the way through the internship. I appreciate their effort of always taking time for me to help and answer questions, which has resulted to an efficient internship experience. This research was carried out at the Jet Propulsion Laboratory, California Institute of Technology, and was sponsored by the Spring 2011 Undergraduate Students Research Program (USRP) and the National Aeronautics and Space Administration.

References

Combes M., and 19 co-authors (1991) Martian Atmosphere studies from the ISM experiment; Planet. Space Sci., 39, 189-197.

Hayes, A.G., Aharonson, O., Callahan, P.,Elachi, C.,Gim, Y.,Kirk, R., Lewis, K., Lopes,R., Lorenz, R., Lunine, J., Mitchell, K., Mitri, G., Stofan, E., and S. Wall (2008) Hydrocarbon lakes on Titan: Distribution and interaction with a porous regolith; Geophys. Res. Lett., 35, L09204, doi:10.1029/2008GL033409.

Hayes, A.G., O. Aharonson, J.I. Lunine, R.L. Kirk, H.A. Zebker, L.C. Wye, R.D. Lorenz, E.P. Turtle, P. Paillou, G. Mitri, S.D. Wall, E.R. Stofan, K.L. Mitchell, C. Elachi, the Cassini RADAR Team (2011) Transient surface liquid in Titan's polar regions from Cassini; Icarus, 211, 655-671.

Le Mouelic S., (2011) Planet. Space Sci., in press.

McCord, T. B., Hansen, G. B., Buratti, B. J., Clark, R. N., Cruikshank, D. P., D'Aversa, E., Griffith, C. A., Baines, E. K. H., Brown, R. H., Dalle Ore, C. M., Filacchione, G., Formisano, V., Hibbitts, C. A., Jaumann, R., Lunine, J. I., Nelson, R. M., Sotin, C., the Cassini VIMS Team, 2006. Composition of Titan's surface from Cassini VIMS. Planet. Space Sci. 54, 1524-1539, doi: 10.1016/j.pss.2006.06.007.

Sobolev V.V. (1975) Light scattering in planetary atmospheres; Pergamon, New York.

Soderblom, L. A., Kirk, R. L., Lunine, J. I., Anderson, J. A., Baines, K. H., Barnes, J. W., Barrett, J. M., Brown, R. H., Buratti, B. J., Clark, R. N., Cruikshank, D. P., Elachi, Ch., Janssen, M. A., Jaumann, R., Karkoschka, E., Le Mouélic, S., Lopes, R. M., Lorenz, R. D., McCord, T. B., Nicholson, Ph. D., Radebaugh, J., Rizk, B., Sotin, C., Stofan, E. R., Sucharski, T. L., Tomasko, M. G., Wall, S. D. (2007b) Correlations between Cassini VIMS spectra and RADAR SAR images: Implications for Titan's surface composition and the character of the Huygens Probe Landing Site. Planet. Space Sci. 55, 13, 2025-2036, doi: 10.1016/j.pss.2007.04.014.

Stephan, K., Jaumann, R., Karkoschka, E., Kirk R.l., Barnes, J.W., Tomasko, M.G., Turtle, E.P., Le Corre, L., Langhans, M., Le Mouelic, S., Lorenz, R.D., Perry, J. (2009) Mapping products of Titan's surface; in "Titan from Cassini Huygens", Brown, R.H. et al. (Eds), Springer, 489-510.

Stiles, B.W., Kirk, R.L., Lorenz, R.D., Hensley, S., Lee, E., Ostro, S.J., Allison, M.D., Callahan, P.S., Gim, Y., Iess, L., Perci del Marmo, P., Hamilton, G., Johnson, W.T.K., West, R.D., and the Cassini RADAR Team (2010) Erratum: "Determining Titan's spin state from Cassini radar images" (2008, AJ, 135, 1669); Astronomical Journal, 139,311.

Stofan, E.R., 37 colleagues (2007) The lakes of Titan. Nature 445, 61–64.

Turtle et al., 2010

Appendix A

Table 1: lakes observed by VIMS cubes during the T69 flyby.

	Diameter	Latitude			Longitude East			Surface area (km2)		
	km	USGS	Radar	VIMS	USGS	Radar	VIMS	USGS	Radar	VIMS
Atitlán Lacus	13.7	69.3	69.3	69.4	121.2	121.2	121.8	147.4	226.1	223.1
Cayuga Lacus	22.7	69.8	69.7	70.0	130.0	130.0	130.3	404.7	297.6	503.7
Lanao Lacus	34.5	71.0	70.9	71.1	142.3	142.3	142.6	934.8	2,408.5	948.0
Logtak Lacus	14.3	70.8	70.8	70.5	133.9	133.9	133.8	160.6	239.9	68.4
Ohrid Lacus	17.3	71.8	71.9	72.3	138.1	138.1	137.8	235.1	286.6	811.7
Sevan Lacus	46.9	69.7	69.7	69.8	134.4	134.4	134.9	1,727.6	843.7	589.0
Uvs Lacus	26.9	69.6	69.6	69.7	114.3	114.6	114.8	568.3	735.7	525.3
Vänern Lacus	43.9	70.4	70.3	70.5	136.9	136.9	137.4	1,513.6	1,411.9	441.2
Freeman				73.6			148.9			430.9
Cardiel				70.2			153.5			462.2
Towada			71.4	71.6		115.8	116.0		491.6	619.3
VIMSNN4				68.0			152.0			

Table 2: New lakes observed by VIMS. The surface area of those lakes in between 400 and 500 km^2. Since they are a few VIMS pixels wide, the uncertainty is quite large and around 200 km^2.

		Latitude		Longitude East		Distance (km)		
		Radar	VIMS	Radar	VIMS	N-S	E-W	Radar
VIMSNN1	Freeman		73.6		148.9	16.0	26.0	
VIMSNN2	Cardiel		70.2		153.5	22.0	21.0	
VIMSNN3	Towada	71.4	71.6	115.8	116.0	32.0	20.0	24 / 20
VIMSNN4			68.0		152.0	16.5	4.2	

Appendix B

The Belet Dunes

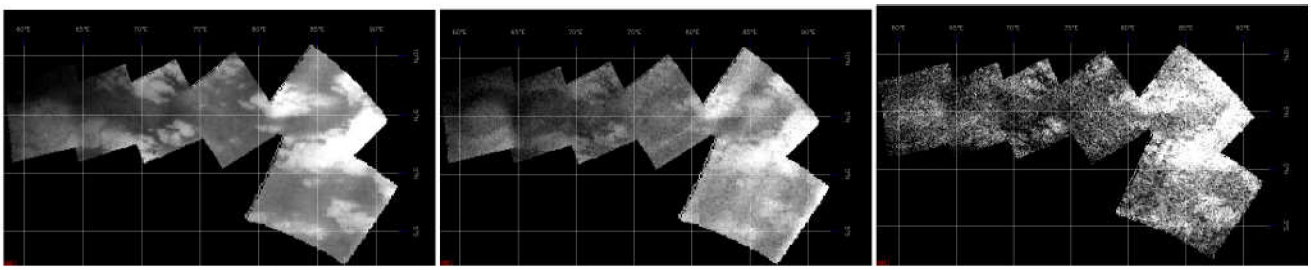

Figure 15. High Resolution Mosaic of Belet Dunes at windows D1(left), D2(center) and D3(right)

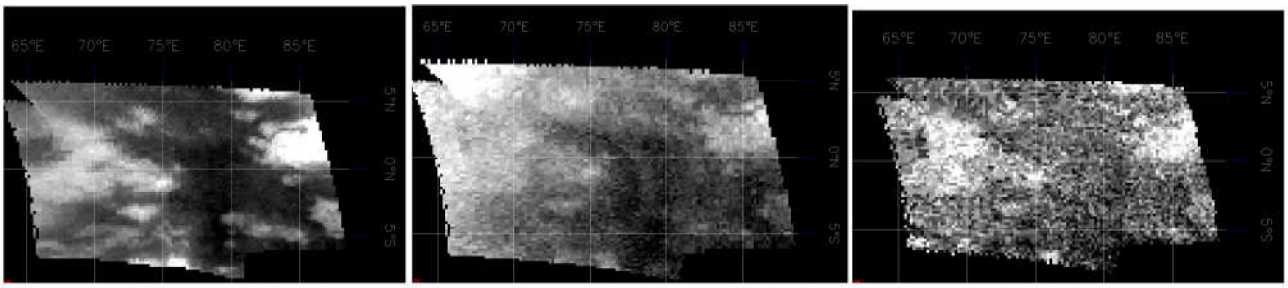

Figure 16. High Resolution Image of Belet Dunes at windows D1(left), D2(center) and D3(right)

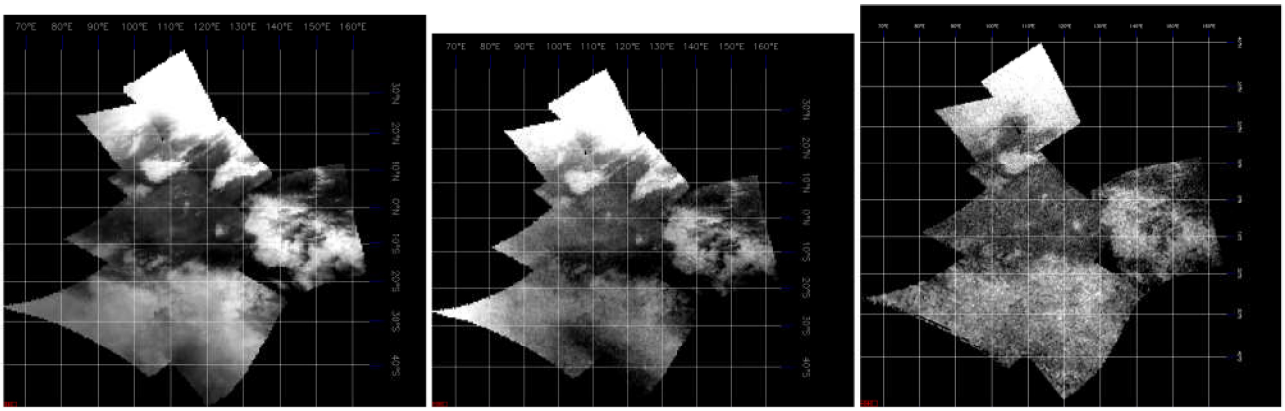

Figure 17. Medium Resolution Mosaic of Belet Dunes at windows D1(left), D2(center) and D3(right)

The Ring Feature

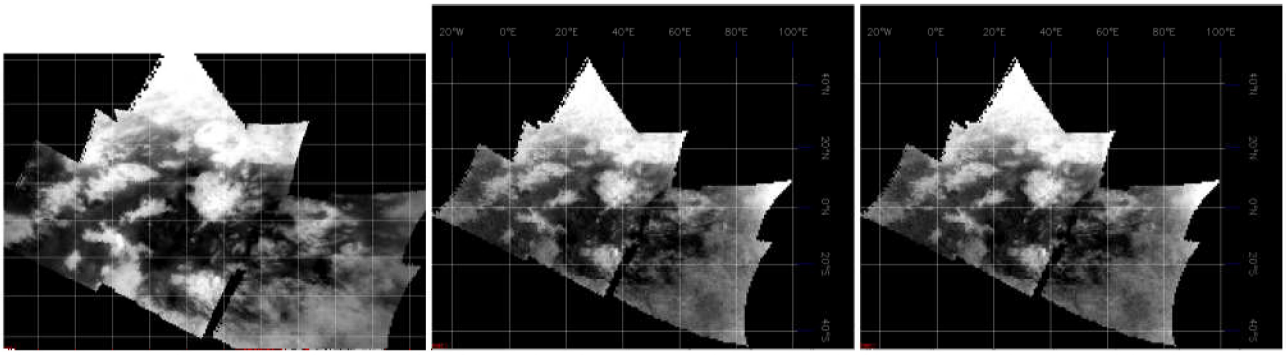

Figure 18. Medium Resolution Mosaic of the Ring feature at windows D1(left), D2(center) and D3(right)

Tortola Facula

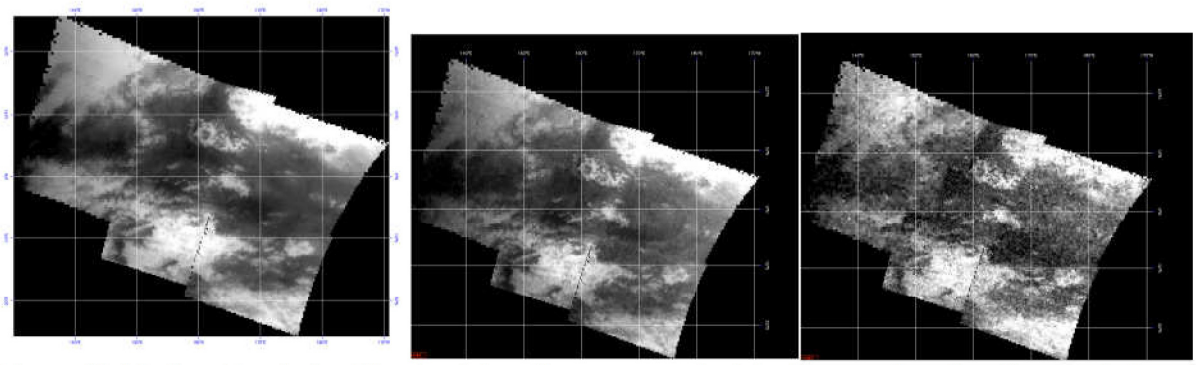

Figure 19. Medium Resolution Mosaic of the selk crater, north of the Huygens Landing Site, at windows D1(left), D2(center) and D3(right)

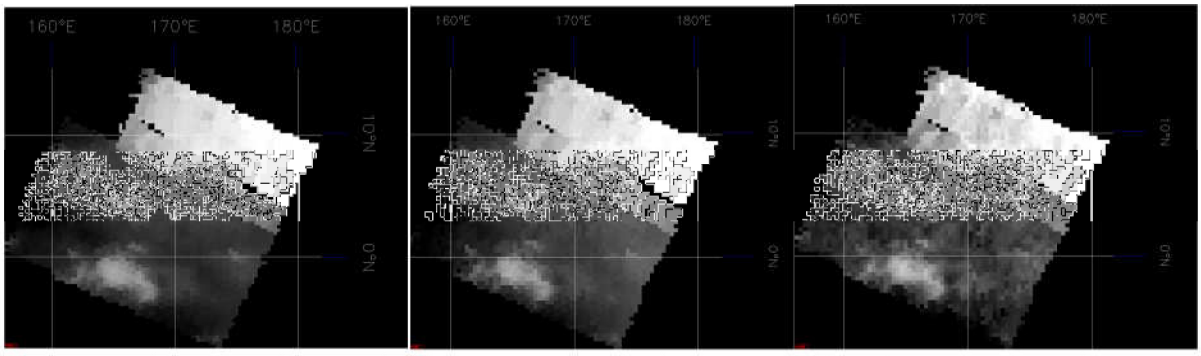

Figure 20. High Resolution Mosaic of Tortola Facula at windows D1(left), D2(center) and D3(right)

Mosaic of Area covered by VIMS

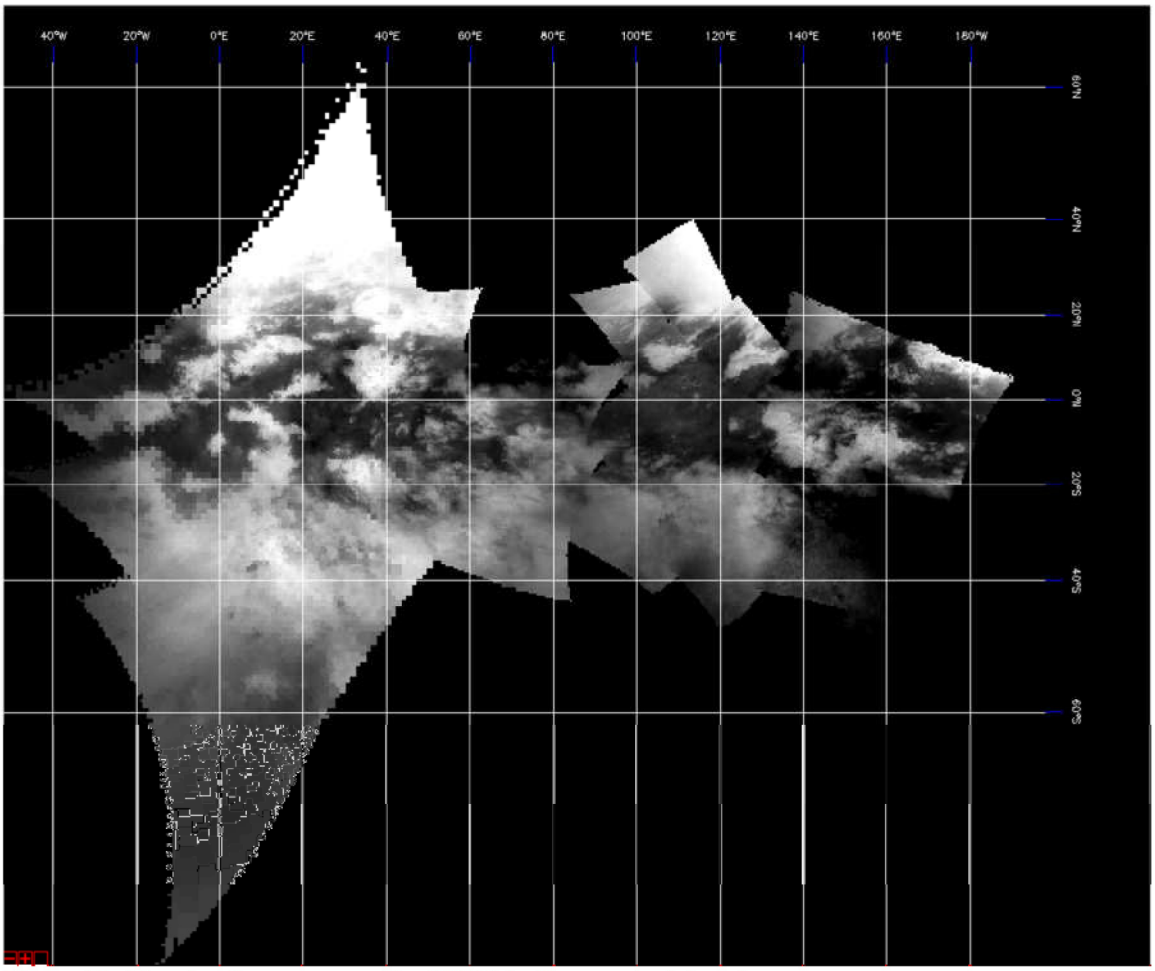

Figure 21. Mosaic of area covered by VIMS in the equatorial region